# Studies on the Northern Early Summer Teleconnection Patterns, Their Interannual Variations and Relation to Drought / Flood in China①

*Shi Neng* (施能) and *Zhu Qiangen* (朱乾根)
Nanjing Institute of Meteorology, Nanjing 210008
Received March 26, 1992; revised July 23, 1992

ABSTRACT

By using the one-point correlation method, calculations have been made of the northern early summer 500 hPa teleconnection patterns. Seven teleconnection patterns are revealed, namely, the Western Atlantic (WA), the Eastern Atlantic (EA), the Eurasian (EU), the Bengal / Northern Pacific (BNP), the Western Pacific (WP), the East Asian / Pacific (EAP), and the Huanghe / East Asian (HEA) patterns. Their centers are determined and their yearly intensity indices (1951-1990) are calculated. On this basis the relationship between their interannual variations and the drought / flood in China is examined. It is noted that the EU, HEA and EAP wave trains are closely related to the drought / flood in China. The HEA and EAP patterns strongly influence the precipitation in eastern China. For example, the fierce floods experienced in 1991 early summer over China are related to the weak EAP and strong HEA patterns.

## I. INTRODUCTION

The atmospheric circulation anomaly has remote correlation. Such discovery can be traced back to the year of 1897, when Hilbebradson noted that the Southern Oscillation (SO), so named later by Walker, was a teleconnection phenomenon of the air pressure field. During the 1980s, Wallace and Gutzler (1981) discovered that there existed five basic teleconnection patterns in Northern winter. Later, Shukla and Wallace (1983), Tokioka et al. (1985), Horel and Wallace (1981) interpreted by numerical experiments that the sea temperature anomaly over the tropical eastern Pacific could produce the Pacific / North American teleconnection (PNA) pattern in the Northern Hemisphere. Recently, Shi Neng and Zhu Qiangen (1992) found after calculating 40 years (1951-1990) of the Northern winter teleconnection intensity indices that when the El Nino or anti-El Nino year develops at its mature stage (winter), the difference in the WP intensity index becomes the most prominent, followed by the PNA. All the anti-El Nino years are the strong WP or weak PNA patterns. The El Nino year at its mature stage is the strong PNA pattern but some of the El Nino years (1951, 1953, 1965 and 1972) are the weak PNA patterns. Such results are of great significance to thorough understanding of the evolution of the atmospheric circulation.

The teleconnection regime shows the wave train features, mainly propagating poleward and eastward. In order to interprete this phenomenon, Hoskins et al. (1981) advanced the so-called great circle theory.

Lots of studies on the teleconnection phenomena have been basically limited to

①This study is one of the research projects sponsored by the Monsoon Research Foundation of State Meteorological Administration.

wintertime. Hardly any covers the northern summer atmospheric circulation teleconnection. As the summer atmospheric circulation variations play an important part in the distribution and maintenance of the monsoon rain belt, and the Mei-yu intensity in China, it is instructive to make thorough and detailed studies on the Northern summer teleconnection characteristics. Recently Huang Ronghui, Chen Lieting et al. have touched in their research the problem of the summer teleconnection. Using the daily 500 hPa disturbance height field data for the Northern 1971-1976 summer, Huang Ronghui has filtered out the high-frequency disturbance on the time scale of less than 10 days and calculated the point correlation coefficient distribution diagram of the Northern summer disturbance height field at the benchmarks of 20 ° N, 120 ° E (Huang Ronghui and Sun Fengying, 1992) and 90 ° E, 30 ° N (Huang Ronghui, 1990), thus finding an atmospheric circulation teleconnection pattern in the region from South Asia through East Asia to North America, which is similar to the PNA pattern and is named the EAP pattern. This teleconnection pattern is in agreement with the result of the secular high cloud amount from satellite observations by Nitta (1987). Chen Lieting and Wu Rengguang (1991) have calculated the east-west pressure oscillation in the Northern Pacific tropics, i.e., the teleconnection of the Northern Oscillation (NO) intensity to the Northern winter / summer atmospheric circulation, believing that the teleconnection has both strong regionality and pronounced seasonal variation. However, the above studies on the summer teleconnection are preliminary and many problems remain to be further investigated. What teleconnection patterns are evidently noted in the Northern summer? Where are their centers? Where should the benchmark be taken in the single-point correlation diagram? What is the intensity of the teleconnection patterns? Can the relationship between the teleconnection patterns and weather / climate be more quantitatively and objectively determined? For these purposes, it is necessary to calculate the teleconnection centers adopting the approach (Wallace and Gutzler, 1981) and using the 500 hPa monthly mean height data so as to determine their patterns. As summer is at the time of the transformation and adjustment of the northern atmospheric circulation and has an important influence on the Mei-yu intensity and the rain belt distribution in China, our study will first focus on the early summer (June) northern circulation.

## II. DATA AND APPROACHES

In this study, 35 years (1951-1985) of the northern 500 hPa June monthly mean height data are used at the grid point of 5 ° latitude × 10 ° longitude (altogether 576 grid points in the Northern Hemisphere). The data come from the long-range weather prediction data base. In calculating the teleconnection intensity index, the Northern-Hemisphere data from 1986 through 1990 are used, taken from the published historical weather atlas and climate monitoring bulletins.

In order to locate the teleconnection centers and classify them, we use the so-called single point correlation method, i.e., calculating

$$r_i = \left| \min_j (r_{ij}) \right| \qquad \begin{matrix} i = 1,2,\cdots,576 \\ j = 1,2,\cdots,576 \end{matrix},$$

which indicates that the teleconnection coefficient at a given grid point is the greatest negative correlation value of the correlation coefficients at the grid point and the other grid points, and then the absolute value is taken. Thus, in calculating the teleconnection patterns, it is necessary to calculate $576^2 = 33176$ correlation coefficients. The high-value center of $r_i$ often exists in pairs and its distribution shows strong regionality so that the teleconnection centers and

their patterns can be easily discovered and defined.

## III. THE NORTHERN EARLY SUMMER 500 hPa TELECONNECTION PATTERNS

Fig. 1 shows the distribution of the teleconnection coefficient ($r_i$), in which the correlation coefficient in the blackened area is $>0.60$, in the double-oblique-line area $>0.55$, and in the single-oblique-line area $>0.5$. The features in the areas indicate that the early summer teleconnection patterns geographically have significant stationary wave oscillation characteristics of node and anti-node. From Fig. 1, three strong, three moderate and one weak early summer 500 hPa teleconnection patterns are given in their proper order:

1. The Western Atlantic pattern (WA): This is a north-south seesaw regime situated in the western Atlantic, composed of meridional dipoles. This pattern is the strongest, reaching −0.70, with its center at A (60 ° N, 60 ° W), B (35 ° N, 45 ° W), as shown in Figs. 2–3. Thus, the early summer WA intensity index is defined as

$$WA = \frac{1}{2}[H^*(60\,^\circ\text{N},\ 60\,^\circ\text{W}) - H^*(35\,^\circ\text{N},\ 45\,^\circ\text{W})],$$

where $H^*$ denotes the standardized 500 hPa height value. It is seen from Fig.1 and the above formula that the large positive value of WA corresponds to the western Atlantic jet, the weak Icelandic low and the weak subtropical high, and vice versa.

2. The Eurasian pattern (EU): This is a roughly southeast-northwest dipole pattern situated in the Eurasian continent. Its central intensity reaches −0.65 with the center at C (50 ° N, 80 ° E), D (65 ° N, 35 ° E). Thus, the corresponding EU intensity index is defined as

$$EU = \frac{1}{2}[H^*(50\,^\circ\text{N},\ 80\,^\circ\text{E}) - H^*(65\,^\circ\text{N},\ 35\,^\circ\text{E})].$$

3. The Bengal-Northern Pacific pattern (BNP): This pattern does not exist in winter. But in summer (June), its intensity reaches −0.65 over vast areas. It runs from northeast to southwest with its center at E of the Pacific (40 ° N, 170 ° E) and of the Bay of Bengal (15 ° N, 85 ° E), hence

$$BNP = \frac{1}{2}[H^*(40\,^\circ\text{N},\ 170\,^\circ\text{E}) - H^*(15\,^\circ\text{N},\ 85\,^\circ\text{E})].$$

This teleconnection pattern indicates that in early summer the Bay of Bengal and the north Pacific shows a seesaw regime.

4. The Western Pacific pattern (WP): This is a north-south seesaw regime situated in the West Pacific. Its intensity is weaker than that in winter, only −0.60, with its center at G (65 ° N, 175 ° E) and H (30 ° N, 170 ° E)

$$WP = \frac{1}{2}[H^*(65\,^\circ\text{N},\ 170\,^\circ\text{E}) - H^*(30\,^\circ\text{N},\ 170\,^\circ\text{E})].$$

The large WP value indicates the weak Aleutian oscillation, the weak west Pacific subtropical high and the weak jet over Japan, and vice versa.

5. The Eastern Atlantic pattern (EA): This is a north-south seesaw regime situated in West Europe and North Africa. Its intensity is rather weak, only −0.55. Its northern end is situated in northwestern Europe, at I (55 ° N, 15 ° E) and its southern end in North Africa, at J (25 ° N, 15 ° E)

$$EA = \frac{1}{2}[H^*(55\,^\circ\text{N},\ 15\,^\circ\text{E}) - H^*(25\,^\circ\text{N},\ 15\,^\circ\text{E})].$$

6. The East Asian / Pacific pattern (EAP): This is the teleconnection pattern discovered by Huang Ronghui from the daily disturbance height field data. Our calculation from the monthly mean height field shows that its intensity is moderate, reaching −0.59. One of its centers is near the Hainan Island in South Asia, at L (20 ° N, 110 ° E) and the other in North America, at K (45 ° N, 125 ° W)

$$EAP = \frac{1}{2}[H^*(45\,^\circ\text{N},\ 125\,^\circ\text{W}) - H^*(20\,^\circ\text{N},\ 110\,^\circ\text{E})].$$

This teleconnection pattern strongly influences the early summer drought / flood distribution over China.

7. The Huanghe / East Asian pattern (HEA): Its intensity is rather weak, only −0.55 at its center. It runs from northeast to southwest. Its southern end is over the Hetao area in China, at N (40 ° N, 110 ° E) and its northern end over Northeast Asia, at M (60 ° N, 120 ° E)

$$HEA = \frac{1}{2}[H^*(60\,^\circ\text{N},\ 120\,^\circ\text{E}) - H^*(40\,^\circ\text{N},\ 110\,^\circ\text{E})].$$

This teleconnection pattern is roughly on the track of the wave train big circle of the EAP pattern (see Fig. 5).

Fig. 2 gives the yearly 500 hPa height value of the seven teleconnection centers, in which the broken-line coordinate is on the right side and the solid-line coordinate on the left. It is seen that they show evident negative correlations, reflecting the above-mentioned seesaw feature.

Fig. 3 is the schematic diagram of the northern 500 hPa teleconnection for June and winter, in which the broken line indicates the winter teleconnection pattern and the solid line the

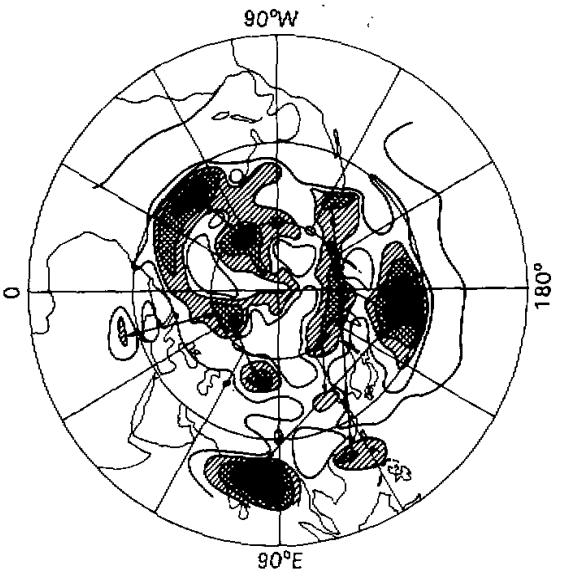


Fig. 1. The northern June 500 hPa teleconnection.

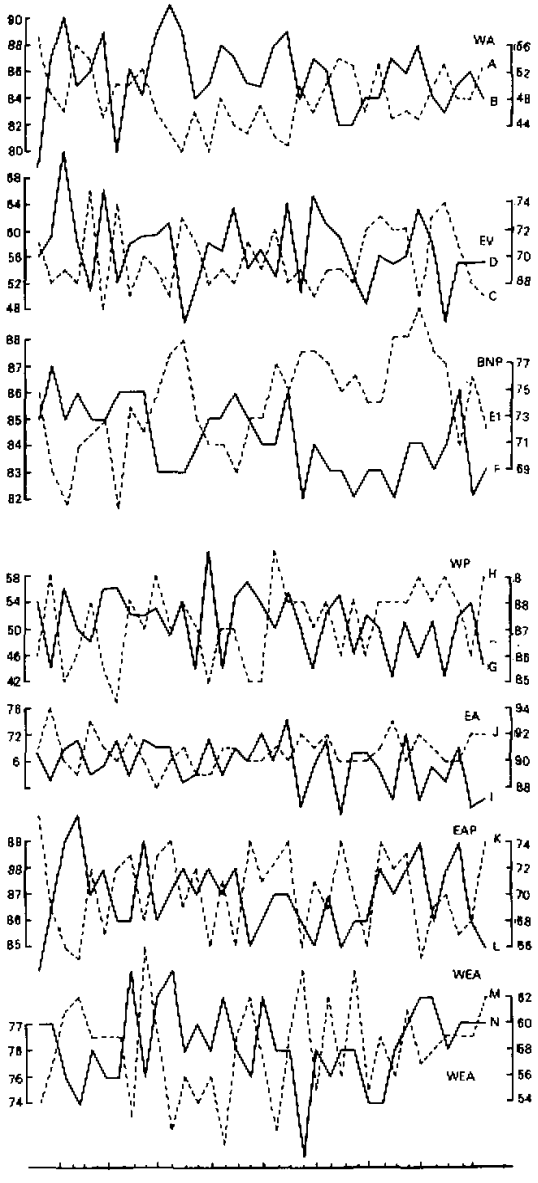


Fig. 2. The northern 500 hPa teleconnection centers' intensity (1951–1985). Unit: geopotential dm (minus 500).

A: (60 ° N, 60 ° W), B: (35 ° N, 45 ° W), C: (50 ° N, 80 ° E), D: (65 ° N, 35 ° E), E:(40 ° N, 170 ° E), F: (15 ° N, 85 ° E), G: (65 ° N, 175 ° E), H: (30 ° N, 170 ° E), I: (55 ° N, 15 ° E), J:(25 ° N, 15 ° E), K:(45 ° N, 125 ° W ), L:(20 ° N, 110 ° E), M: (60 ° N, 120 ° E), N:(40 ° N, 110 ° E)

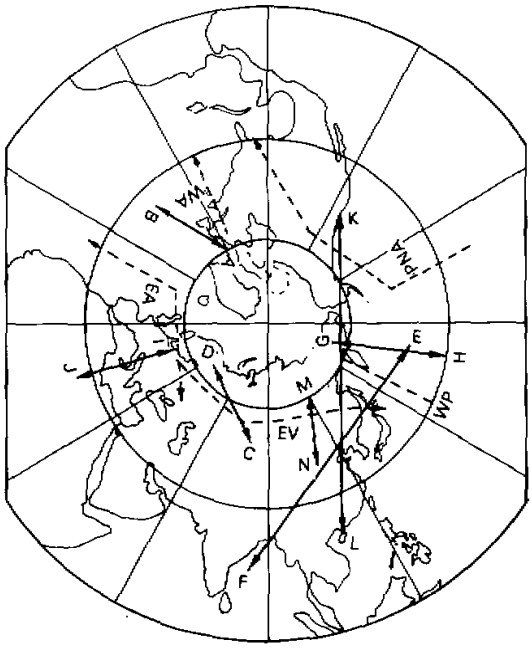


Fig. 3. The schematic diagram of the northern 500 hPa winter (broken line) and early summer (solid line) teleconnection.

seven June teleconnection patterns. It is seen that the differences between the early summer teleconnection and the winter teleconnection are:

1) The winter WP, EA and WA patterns have moved eastward in their location at least 15 ° longitude in early summer and the southern ends of the WA and WP patterns even farther.

2) The EU pattern can propagate to the Sea of Japan in winter but only to 90 ° E in early summer, replaced by the north–south HEA pattern at its eastern end.

3) The PNA pattern which is noticeable in winter does not exist in early summer, replaced by the similar EAP pattern.

4) The early summer BNP pattern does not occur in winter.

## IV. THE ANNUAL VARIATIONS OF THE TELECONNECTION PATTERNS AND THEIR INTENSITY INDICES

In order to know the annual variations of the teleconnection patterns, we have calculated the yearly values of the seven early summer teleconnection patterns in terms of the teleconnection index formula defined above, as shown in Table 1. As they are the linear combinations of the standardized variables, the secular mean values of the indices of the patterns are all zero.

Table 2 shows the mean square deviations of the teleconnection intensity indices in winter months. Comparison of Fig. 1 with Fig. 2 shows that the WA, WP, EA and EU patterns are not weak in early summer and their interannual variations are also evident.

**Table 1.** The Yearly Values, Means and Mean Square Deviations (1951–1985)

| Year \ Pattern | WA | WP | EA | EU | BNP | HEA | EAP |
|---|---|---|---|---|---|---|---|
| 51 | 2.32 | 0.75 | 0.20 | 0.38 | −0.13 | −0.92 | 2.09 |
| 52 | −0.09 | −1.25 | −1.46 | −0.50 | −1.72 | −0.49 | 0.18 |
| 53 | −0.99 | 1.46 | 0.71 | −1.45 | −1.26 | 0.77 | −1.44 |
| 54 | 1.06 | 0.26 | 1.22 | −0.41 | −1.06 | 1.26 | −1.98 |
| 55 | 0.65 | −0.54 | −0.95 | 1.64 | −0.55 | 0.14 | 0.30 |
| 56 | −0.91 | 1.34 | −0.07 | −1.54 | −0.41 | 0.49 | −0.90 |
| 57 | 1.37 | 1.68 | 0.85 | 1.35 | −1.77 | 0.49 | 0.68 |
| 58 | 0.21 | −0.17 | −0.58 | −0.62 | −0.64 | −1.75 | 0.84 |
| 59 | 0.82 | 0.17 | 0.85 | −0.09 | −0.92 | 1.48 | −1.11 |
| 60 | −0.80 | −0.39 | 1.46 | −0.30 | 0.61 | −0.55 | 0.84 |
| 61 | −1.51 | −0.20 | 0.71 | −0.89 | 1.04 | −1.89 | 0.63 |
| 62 | −1.45 | 0.07 | −0.34 | 1.68 | 1.18 | −0.29 | −0.57 |
| 63 | 0.16 | −0.57 | 0.54 | 0.82 | −0.04 | −0.92 | 0.30 |
| 64 | −0.69 | 2.07 | 1.22 | −0.41 | −0.69 | −0.29 | −1.06 |
| 65 | −0.39 | −0.57 | −0.21 | −0.12 | −0.69 | −1.69 | 0.14 |
| 66 | −0.63 | 0.54 | 0.34 | −0.86 | −1.35 | 0.14 | −1.06 |
| 67 | −0.36 | 1.46 | 0.44 | 0.56 | −0.41 | 0.91 | 1.38 |
| 68 | 0.08 | 1.09 | 0.99 | −0.12 | −0.04 | −0.84 | 0.51 |
| 69 | −1.04 | −1.10 | 0.07 | 0.85 | 0.52 | −0.85 | 0.30 |
| 70 | −1.34 | 0.20 | 1.26 | −0.95 | −0.50 | 0.14 | 0.63 |
| 71 | 0.60 | −0.42 | −1.26 | 0.41 | 1.40 | 2.24 | −0.31 |
| 72 | −0.41 | −0.57 | −0.07 | −1.24 | 0.67 | −0.43 | 0.89 |
| 73 | 0.21 | −0.05 | 0.10 | −0.48 | 0.89 | 0.91 | −0.19 |
| 74 | 1.42 | 0.88 | −0.65 | −0.30 | 0.61 | −0.29 | 1.38 |
| 75 | 1.31 | −0.66 | 0.58 | 0.03 | 1.12 | 0.85 | 0.35 |
| 76 | 0.16 | 0.51 | 0.58 | 1.21 | 0.47 | 0.27 | −0.31 |
| 77 | 0.93 | −0.42 | −0.07 | 0.79 | 0.47 | 0.83 | 0.26 |
| 78 | −0.52 | −1.03 | −1.50 | 0.67 | 1.55 | −0.29 | 0.30 |
| 79 | −0.22 | −0.29 | 0.99 | 0.58 | 0.81 | 0.08 | 0.09 |
| 80 | −0.71 | −1.00 | −1.13 | −1.06 | 0.95 | −0.84 | −1.60 |
| 81 | 0.49 | −0.29 | −0.07 | 0.61 | 0.75 | −0.69 | 0.18 |
| 82 | 1.12 | −1.37 | 0.03 | 1.88 | 0.24 | 0.14 | −0.40 |
| 83 | 0.19 | −0.17 | 0.71 | 0.47 | −1.35 | −0.21 | −1.27 |
| 84 | −0.00 | 0.75 | −1.26 | −0.15 | 1.12 | 0.14 | 0.02 |
| 85 | 0.93 | −1.12 | −1.40 | −0.35 | 0.18 | 0.57 | 1.38 |
| 86 | −1.48 | −0.48 | 0.61 | −1.65 | 0.24 | 0.71 | 0.35 |
| 87 | 0.71 | −1.37 | −1.64 | −0.00 | 0.58 | −0.35 | −0.90 |
| 88 | −0.82 | −0.42 | −0.92 | −0.13 | −1.21 | −0.49 | −0.73 |
| 89 | 0.54 | 0.69 | −0.31 | −1.10 | −0.55 | 0.22 | 0.09 |
| 90 | −0.91 | 0.51 | −0.58 | 0.79 | −0.10 | 1.26 | −0.36 |
| Mean value | 0.0 | 0.0 | 0.0 | 0.0 | 0.0 | 0.0 | 0.0 |
| Mean square deviation | 0.91 | 0.87 | 0.86 | 0.90 | 0.89 | 0.88 | 0.88 |

**Table 2.** The Mean Square Deviations of the Winter Teleconnection Intensity Indices

| Pattern / Month | PNA | WA | WP | EA | EU |
|---|---|---|---|---|---|
| Dec. | 0.78 | 0.88 | 0.92 | 0.76 | 0.75 |
| Jan. | 0.83 | 0.81 | 0.87 | 0.79 | 0.86 |
| Feb. | 0.83 | 0.88 | 0.87 | 0.78 | 0.79 |

Table 3 shows the correlation matrixes of the seven early summer teleconnection patterns. It is seen that the linear correlation coefficients between these patterns are all small, indicating that the classified teleconnection patterns are unequal (those between the WP, EA and BNP patterns and between the WA and EU patterns are slightly larger).

**Table 3.** The Correlation Coefficients of the Teleconnection Patterns Calculated from 40 Years of Data

| Pattern | WP | EA | EU | BNP | HEA | EAP |
|---|---|---|---|---|---|---|
| WA | −0.02 | −0.12 | 0.34 | −0.06 | 0.21 | 0.24 |
| WP | | 0.46 | −0.16 | −0.36 | 0.20 | −0.03 |
| EA | | | −0.08 | −0.25 | 0.05 | −0.05 |
| EU | | | | 0.15 | 0.06 | 0.12 |
| BNP | | | | | | 0.23 |
| HEA | | | | | | −0.28 |

By using the yearly values of the teleconnection intensity indices in Table 1, we can study quantitatively the relation between these indices and the world weather / climate.

## V. THE RELATIONSHIP BETWEEN THE EARLY SUMMER TELECONNECTION PATTERNS AND DROUGHT / FLOOD IN CHINA

In order to study the relation between the teleconnection patterns and drought / flood in China, we have determined the correlation between the teleconnection intensity indices given in Table 1 and the precipitation sequence in June by using the data from 160 weather stations. Table 4 gives the number of stations (out of the 160 stations) with correlation coefficients reaching confidence more than 0.05. It is found that the EU, EAP and HEA patterns are closely related to the early summer precipitation in China.

**Table 4.** The Seven Teleconnection Patterns and the Number of the Stations (out of 160) with June precipitation correlation reaching confidence more than 0.05

| Pattern | WA | EA | EU | WP | EAP | HEA | BNP |
|---|---|---|---|---|---|---|---|
| Number of stations | 12 | 13 | 36 | 12 | 27 | 38 | 6 |

### 1. *The Effect of the EU Pattern on Drought / Flood in China*

Fig. 4 is the one-point diagram of the benchmark at (50 ° N, 80 ° E) (C in Fig. 3), in which the solid line indicates positive values and the broken line negative values, the interval being 0.1 (from 0.7 to −0.6). It can be seen that the Eurasian continent is a very strong negative correlation area. There are wave train structures at 50 ° N and China's mainland south of 40 ° N is the area of negative correlation. It is known from the formula for the EU pattern that when the EU pattern is strong, the 500 hPa height decreases over China south of 40 ° N

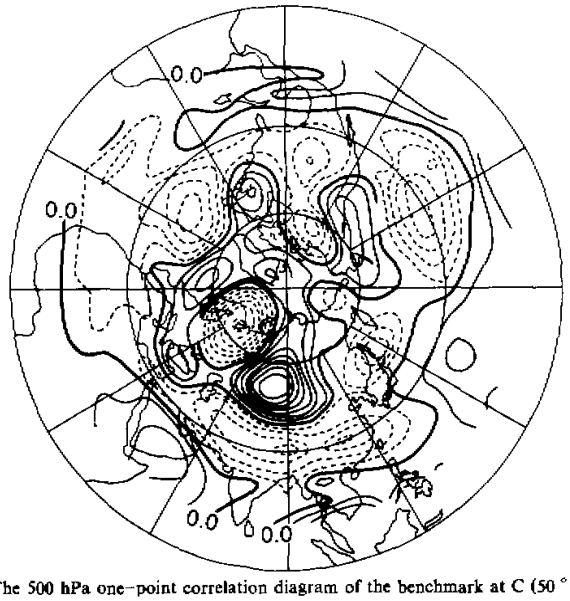


Fig. 4. The 500 hPa one-point correlation diagram of the benchmark at C (50 ° N, 80 ° E) (the EU pattern in June).

and the negative center is observed over the middle reaches of the Changjiang River. Such characteristics of the height field indicate that precipitation will be scarce over China in June.

By determining the correlation between the EU intensity index and the precipitation at the 160 stations, we find that 101 stations show negative correlation. There are 36 stations with correlation reaching confidence more than 0.05 (among them 25 stations have negative correlation). The correlation distribution (omitted) shows weak positive correlation south of the Changjiang River and north of 40 ° N, and negative correlation in between. The greatest negative correlation is found in southern Shaanxi and northeastern Sichuan (see Table 5), and no significant correlation is observed in the middle and lower reaches of the Changjiang River.

**Table 5.** The EU Intensity Indices and Stations having Close Precipitation Correlation in China (Absolute Values > 0.40)

| | |
|---|---|
| Positive correlation | *Bijie* (0.43), *Lincang* (0.41), *Rongjiang* (0.40) |
| Negative correlation | Xiqinzhen (−0.53), Dongtai (−0.49), Xi'an (−0.46), Chengdu (−0.44), Hanzhong (−0.43), Lanzhou (−0.41), Yanan (−0.41), Mianyang (−0.43) |

2. *The Relation between the HEA Pattern and Drought / Flood in China*

Fig. 5 is the one-point diagram of the benchmark at (40 ° N, 110 ° E), (N in Fig. 3), which shows that there is a north-south seesaw regime near 110 ° E, 40 ° N and 60 ° N. It is seen from the HEA intensity index formula that when the HEA pattern is strong the 500 hPa height decreases over China, thus causing excessive rainfall.

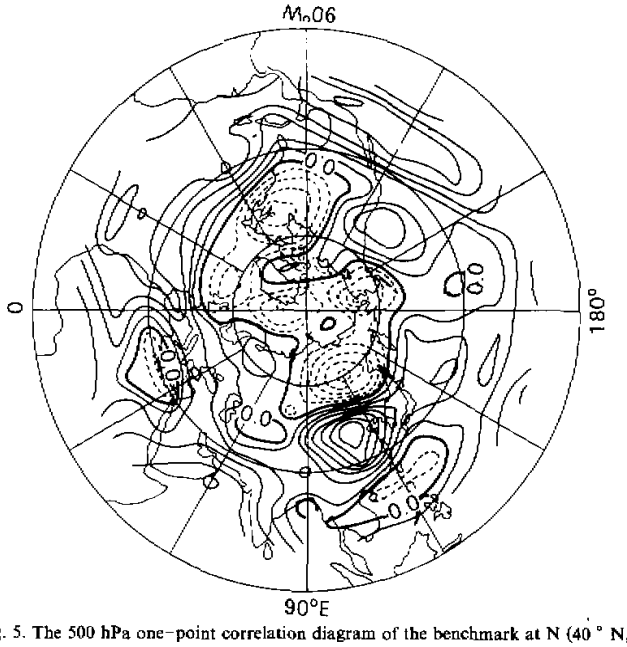


Fig. 5. The 500 hPa one-point correlation diagram of the benchmark at N (40 ° N, 110 ° E) (the WEA pattern in June).

Fig. 6 shows the correlation between the HEA intensity index and the precipitation at the 160 stations in June in China. In the figure, the solid line denotes the positive correlation area (124 stations), the broken line the negative correlation area, the hatched area $>0.30$, and the blackened area $>0.40$. Table 6 gives the 20 stations with correlation coefficient absolute value more than 0.40. It is seen that there is very high positive correlation between the HEA intensity index and Inner Mongolia, the western part of Northeast China, the lower reaches of the Changjiang River, the northern part of North China, central Henan, and Jiangxi, an important factor for drought / flood over the Changjiang River and the vast areas to its north.

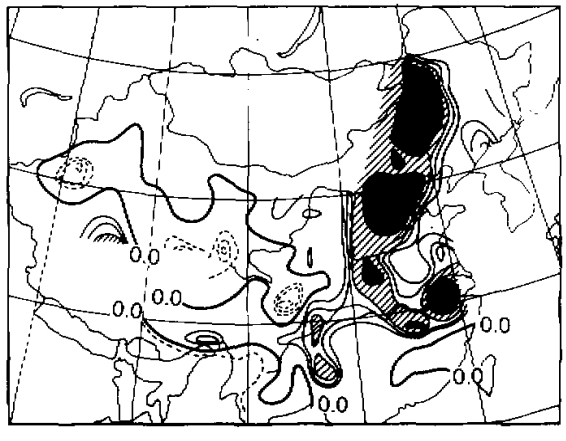

Fig. 6. The correlation between the HEA teleconnection pattern and the 160 stations in China (June).

**Table 6.** The HEA Intensity Indices and Stations Having Close Precipitation Correlation in China (Absolute Values > 0.40)

| Area | Station |
|---|---|
| Inner Mongolia<br>Western NE China | Ulan Hot (0.69), Lindong (0.56), Xilin Hot (0.47)<br>Hailar (0.46), Chifeng (0.42), Bugt (0.43) |
| North China | Beijing (0.56), Tianjin (0.54), Xingtai (0.51),<br>Shijiazhuang (0.51), Dezhou (0.50), Zhangjiakou (0.43),<br>Taiyuan (0.40), Qu Xian (0.40), Changzhi (0.40),<br>Nanyang (0.44) |
| Lower reaches of the<br>Changjiang River | Anqing (0.41), Nanjing (0.43), Tunxi (0.54) |
| Others | Nanchang (0.45) |

3. *The Relation between the EAP Pattern and Drought / Flood in China*

Fig. 7 is the 500 hPa one-point diagram of the benchmark at L (20 ° N, 110 ° E), in which the solid line indicates positive correlation and the broken line negative correlation, the interval being 0.1 (from −0.4 to 0.7). It is found that when positive anomaly is observed at L in South Asia, negative anomaly occurs over North China; when positive anomaly in Siberia, negative anomaly over the sea of Okhotsk and Kamchatka Pen.; when positive anomaly over Alaska and to its west, negative anomaly in the western part of the United States. The greatest negative correlation reaches −0.59, seeming like a quasi-stationary planetary wave train, represented by the heavy solid line with an arrow. The positive value of the EAP pattern denotes positive anomaly over western North America and negative anomaly over South Asia; its negative value denotes negative anomaly over North America and positive anomaly over South Asia.


Fig. 7. The 500 hPa one-point correlation diagram of the benchmark at L (20 ° N, 110 ° E) in South Asia (June).

Fig. 7 also shows that most part of China is within the high correlation area so it is possible to infer the close relation between the EAP pattern and the weather in early summer in China. Fig. 8 shows the precipitation correlation in June between the EAP intensity index and the 160 stations in China, in which the meanings of the lines are the same as in Fig. 6. It is seen from Fig. 7 that there is high negative correlation between the EAP intensity index and the stations in eastern China. Calculation shows that 120 (out of 160) stations show negative correlation, concentrated east of 103 ° E. It follows that the strong EAP pattern corresponds to drought and the weak EAP pattern to flood in eastern China during June. Table 7 gives the close precipitation correlation between the EAP intensity index and the stations (the absolute value is greater than 0.40).

**Table. 7.** The EAP Intensity Indices and Stations Having Close Precipitation Correlation in China (Absolute Values $>0.40$)

| Area | Station |
|---|---|
| North China | Jinan (−0.44), Nanyang (−0.48), Tianjin (−0.40), Chengde (−0.58), Beijing (−0.43), Yantai (−0.44) |
| Middle and lower reaches of the Changjiang River | Hankou (−0.51), Changde (−0.43), Anqing (−0.49), Yueyang (−0.41), Nanchang (−0.40), Tunxi (−0.49) |

It is seen from Fig. 8 and Table 7 that there is a close relation between the EAP pattern and the concurrent drought / flood over the valley of Changjiang River and Huanghe River.

Now let us consider the combined effect of the EAP and HEA patterns. Fig. 9 is the mean precipitation scatter diagram in June of the EAP and HEA patterns and the five stations (Wuhan, Jiujiang, Anqing, Nanjing and Shanghai) over the middle and lower reaches of the Changjiang River. In the figure, the large dark circle denotes wet year (more than 240 mm), the large open circle dry year (less than 162 mm), and the small dark circle normal year. It is seen that the EAP and HEA patterns can diagnose very well the drought / flood over the middle and lower reaches of the Changjiang River. In the figure, the year on the upper left

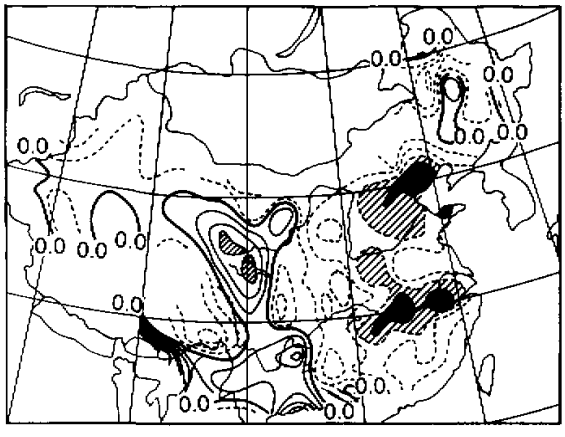


Fig. 8. Correlation between the EAP teleconnection intensity index and the 160 stations in China.

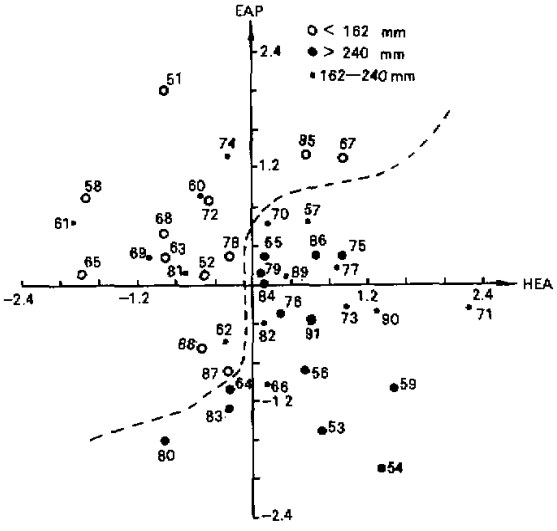


Fig.9. The scatter diagram showing the EAP and HEA patterns and the June precipitation over the middle and lower reaches of the Changjiang River 1951–1990 (1991 is the independent sample).

above the dashed line has rainfall less than 201 mm and the year on the lower right has rainfall more than 167 mm. It is noteworthy to point out that if the scatter diagram had been prepared from Tables 6–7, the diagnostic results would have been better.

In 1991, the middle and lower reaches of the Changjiang River experienced fierce floods. From the 1991 June 500 hPa height, we have calculated: EAP = −0.35, HEA = 0.621,① both indicating rainfall more than normal, as shown in Fig. 9. Thus, the EAP and HEA intensity has high accuracy in diagnosing rainfall.

## V. CONCLUDING REMARKS

1. There exist seven teleconnection patterns in the northern early summer, i.e., the WA, EA, EU, WP, EAP, BNP and HEA patterns, of which the WA, EU and BNP have strong intensity.

2. The teleconnection patterns all have significant variations. The centers of the WA, EA, EU and WP patterns have moved about 15 ° longitude as compared in winter. The PNA pattern is not noticeable in early summer.

3. Very good correlation is found between the EU, EAP and HEA patterns and the concurrent drought / flood in China. When the EAP pattern is strong, drought occurs over North China and the middle and lower reaches of the Changjiang River, and vice versa. When the HEA pattern is strong, flood is experienced over Inner Mongolia, western NE China, North China and the middle and lower reaches of the Changjiang River, and vice versa. The interannual variation of the EU pattern has strong influence on the precipitation over Shaanxi and Sichuan provinces.

4. As there is no close correlation between the EU, EAP and HEA patterns, the

①EU = 0.0 in June, 1991.

interannual variations of the June monsoon rainfall in China can be interpreted from the interannual variation of the teleconnection patterns. The strong HEA and weak EAP patterns are the cause of the fierce floods occurring over the middle and lower reaches of the Changjiang River in June, 1991.

5. In studying the interannual variations of drought / flood, it is necessary to examine from the 500 hPa height field the interannual variations of the EU, EAP and HEA patterns. As one of the EAP teleconnection points is at (20 ° N, 110 ° E), its intensity may be related to the convective activities over the warm pool. This problem remains to be further researched.

REFERENCES

Huang Ronghui and Sun Fengying (1992), Annual variations of Northern summer teleconnection patterns and their numerical simulation, *Scientia. Atmospherica Sinica*, 16 (1): 152-161 (in Chinese).

Horel, J. D. and J. M. Wallace (1980), Planetary-scale atmospheric phenomena associated with the Southern Oscillation, *Mon. Wea. Rev.*, **109:** 813-829.

Hoskins, B. J. and D. J. Karoly (1981), The steady linear response of a spherical atmosphere to thermal and orographic forcing, *J. Atmos. Sci.*, **38:** 1179-1196.

Nitta, T. S. (1987), Convective activities in the western tropical Pacific and their impact on the Northern Hemisphere summer circulation, *J. Meteor. Soc. Japan*, **65:** 373-390.

Shukla, J. and J. M. Wallace (1987), Numerical simulation of the atmospheric response to equatorial sea surface temperature anomalies, *J. Atmos. Sci.*, **40:** 1613-1630.

Tokioka, T.K., Yamazaki and M. Chiba (1985), Atmospheric response to the sea surface anomalies observed in early summer of 1983: a numerical experiment, *J. Meteor. Soc. Japan*, **63:** 565-588.

Wallace, J.M. and D.S. Gutzler (1981), Teleconnections in the geopotential height field during the Northern Hemisphere winter, *Mon. Wea. Rev.*, **109:** 784-812.

Wu Renguang and Chen Lieting (1991), Teleconnections between Northern Oscillation and the Northern Hemisphere extratropical atmospheric circulation: II. seasonal variations, *Scientia Atmospherica Sinica*, 15(6): 36-45 (in Chinese).

Yeh Tucheng and Huang Ronghui (1990), Advances in drought-flood climate research, China Meteorological Press. 37-49 (in Chinese).

Zhu Qiangen and Shi Neng, Variations in the teleconnection intensity index and its remote response to El Nino in the Northern Hemisphere (to be published in A.M.S. Vol. 6 No. 4, 1992).